Chapter 12

Structural Seismic Input Model on the Condition of Slope Site

Li Jianbo and Liu Weihong

Additional information is available at the end of the chapter

http://dx.doi.org/10.5772/intechopen.76619

Abstract

The viscoelastic artificial boundary model is widely used in the field of earthquake resistance analysis of water conservancy projects and nuclear power stations. However, for the analysis of soil-structure dynamic interaction on the sloping site, some problems will arise while using that method. The large size difference of side facades on the outer boundary will cause inconsistent horizontal seismic forces, which may lead to the divergent results or the drift of displacement. In this chapter, based on the basic formula of dynamic interaction and seismic input mechanism, a virtual symmetrical substructure system is built to solve those problems, which not only satisfies the consistence of the whole seismic input on the outer boundary but also simulates the seismic wave propagation. Finally, the accuracy and the stability of the new method are verified through numerical examples on the sloping site.

Keywords: slope site, structure-foundation interaction, viscoelastic boundary, symmetrical substructure, virtual symmetric substructure

1. Introduction

With the development of numerical methods, the advanced dynamic model of infinite foundation [1, 2] is widely used in the field of earthquake resistance analysis of water conservancy projects and nuclear power stations. Now, the viscous boundary [3], viscoelastic boundary [4] and transmitting boundary [5, 6] are more prevalent in engineering. Among them, the viscous boundary is the earliest applied, but it only reflects the energy absorbing effect of boundary damping; under the static or slow dynamic loading, the overall structure drift easily occurs. The transmitting boundary [7, 8] is more accurate, but it cannot reflect the elastic supporting effect of the far-field foundation, and similar to the viscous boundary, the numerical result

drifts easily under the combination of static and dynamic forces; moreover, the problem of high-frequency instability is obvious which limits its application in engineering to a certain extent. In contrast, the viscoelastic boundary [9, 10] can not only effectively simulate the elastic recovery properties and the radiation damaging effect of the medium outside the artificial boundary [11] which ensures the numerical stability and precision that fulfills the requirements of engineering but implement in large software and achieve computational efficiency that endures broad application prospects.

1.1. The research of the viscoelastic artificial boundary

As a stress topical artificial boundary, the viscoelastic artificial boundary gave rise to the artificial boundary condition by Deeks [12] based on the assumption that the two-dimensional scattered wave is cylindrical wave. Liu Jingbo [13] introduced the conversion of the ground motion input into the equivalent load form on the artificial boundary which can deal with the problem of oblique incidence. Later, Liu Jingbo deduced the three-dimensional viscoelastic artificial boundary condition based on the assumption of the scattering wave as a spherical wave and established a three-dimensional viscoelastic static and dynamic unified artificial boundary [10] for static and dynamic combination analysis. Du Xiuli et al. applied the viscoelastic artificial boundary to the analysis of the seismic response of the camber and compared the analysis results of the transmitting boundary method. Lu Huaxi et al. [14] used the viscoelastic artificial boundary to study the interaction of pile foundation structures considering the dynamic nonlinear properties of soil. Gao Feng et al. [15] studied the method of static and dynamic artificial boundary transformation of underground structures and recommended a reasonable method. The viscoelastic artificial boundary is studied and developed for more complex and practical engineering applications.

1.2. The viscoelastic artificial boundary model under the condition of the slope site

Earthquake is an important threat to the safety of engineering structures, which is a natural phenomenon with serious consequences. The analysis of soil-structure dynamic interaction is an important basic method to evaluate reasonable and reliable structures such as engineering structures. The viscoelastic artificial boundary foundation model with good engineering applicability and computational robustness is a widely used model of interaction analysis in the engineering field. How to define the input ground vibration of the viscoelastic artificial boundary foundation model [16] is the basic calculation condition, which is not only related to the seismic event but also involves the dynamic analysis of the ground motion field of the free field. This chapter puts forward the reasonable solution to promote the viscoelastic artificial boundary model applied in the field of large engineering structures for more site conditions of slope soil-structure interaction input conditions and analysis. This slope site condition is often encountered in the seismic analysis of large seawalls, slope protection and water diversion structures. Due to limitations on space, the sketch is described in the example.

In the actual engineering seismic response analysis, the viscoelastic boundary is generally divided into five steps: a system composed of intercepting straight artificial boundaries on the foundation and structure, finite element discretization, applying artificial boundaries, equivalent

http://dx.doi.org/10.5772/intechopen.76619

load generation and input and dynamic time history analysis. For the structure built on a flat field, the height of each lateral face of the foundation model intercepted is generally equal, and the generation and input of equivalent loads are issued [7]. However, there are often slope sites in engineering, such as in the northeast, the water intake structures of a nuclear power plant are built in the gentle slope of the coastal zone where the terrain is in a slope overall. After checking the overall stability of the slope site structure, the viscoelastic artificial boundary is adopted to analyze seismic responses of structures. Intercepting the straight boundary that leads to a matrix as shown in **Figure 1**, this model is characterized by setting different heights of the lateral face. This difference causes two obvious problems for equivalent load generation and direct application: the traveling wave effect with different time delay between the incident and reflected wave causes different displacement time history and stresses of wave propagation in lateral faces with different heights and the resultant force of seismic load relates to the area, area difference of the boundary face which causes different resultants with each side making the force on its side illogical. In fact, the limited model causes problems. The actual source is far away from the surface, so the fluctuation of the surface of the ground does not make a significant difference in the input of the seismic waves. There is no discussion on the method of seismic wave input for slope site in present literature.

In this chapter, based on the basic formula of dynamic interaction and seismic input mechanism, we overcome this problem that the seismic load input is consistent between lateral faces with different heights. A method existing nominally of only an equal-sized slope foundation composing of slope symmetry system with the original slope model is adopted. A virtual symmetrical substructure system is built to solve those problems, which not only satisfies the consistency of the whole seismic input on the outer boundary but also simulates the seismic wave propagation. Finally, the accuracy and the stability of the new method are verified through numerical examples on the sloping site.

With the application of the finite element analysis technique, the classical viscoelastic artificial boundary model has been developed and improved, and its accuracy and applicability have been verified by Liu Jingbo [9, 10, 17], Du Xiuli et al. [7]. The model proposed in this chapter is to solve the input conditions under the conditions of the slope site by defining the virtual interaction analysis model and then obtain the dynamic response of the structure. In this chapter, the theses of Liu Jingbo [9, 10, 17] and Du Xiuli [7] are quoted in this chapter, which

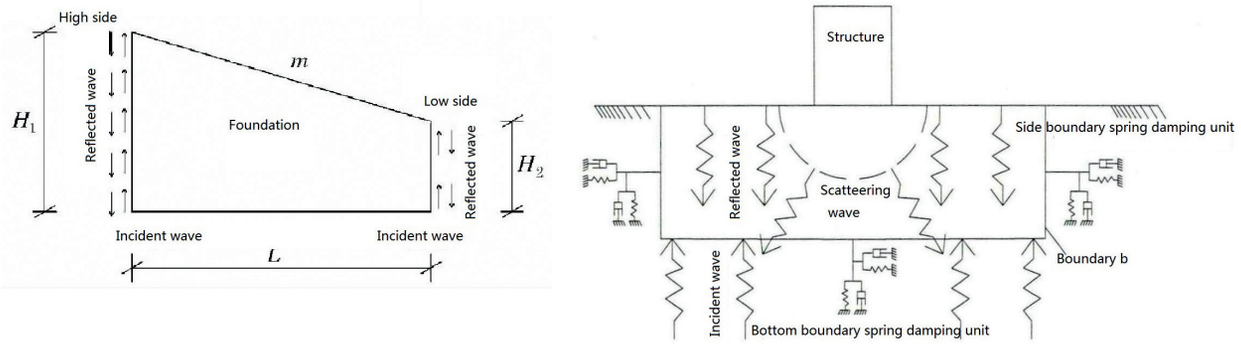

Figure 1. (1) Abstract sketch of slope site model. (2) The sketch of structure-foundation interaction.

mainly refer to the model of input ground vibration in the slope field of this chapter, which conforms to the basic assumption of the viscoelastic artificial boundary model. On this basis, the new model extends the applicability of the viscoelastic artificial boundary model and does not affect its accuracy.

2. The theory of viscoelastic artificial boundary

As shown in **Figure 1 (2)**, the spring damping element is applied to the outer boundary of the topical foundation that is intercepted; the wave from the bottom into the structure foundation system arrives at a time later at the structure, causing structural vibration, and the vibration will also be sent back to the foundation in the form of waves, which is called secondary scattering field fluctuation [18, 19]. So, the vibration of a point on the foundation contains the superposition of three forms of waves: the free field incident wave, the free field reflection wave and the scattered wave of the secondary scattering field. It is assumed that the scattered field wave is divided into cylindrical spherical and waves, respectively, that obtain two- and three-dimensional spring damper coefficients. The specific derivation process can be referred to in the literature [9, 10]. An example of a two-dimensional compressional wave (P-wave) is given here to illustrate the derivation process.

2.1. Formula derivation

Assuming the plane strain condition, the wave front is the cylindrical wave by the example of P-wave; the wave equation of radial displacement is:

$$\frac{\partial^2 u}{\partial t^2} = \frac{2G+\lambda}{\rho}\left(\frac{\partial^2 u}{\partial r^2} + \frac{1}{r}\frac{\partial u}{\partial r} - \frac{u}{r^2}\right) \tag{1}$$

$$\lambda = \frac{\mu E}{(1+\mu)(1-2\mu)} \tag{2}$$

where u is the radial displacement, G is the shear modulus of material at the boundary, λ is *Lamb* constant, E is Young's modulus and μ is Poisson's ratio.

According to the physical and geometric equation, we can obtain:

$$\sigma_\theta = \lambda\varepsilon_r + (2G+\lambda)\varepsilon_\theta \tag{3}$$

$$\sigma_r = \lambda\varepsilon_\theta + (2G+\lambda)\varepsilon_r \tag{4}$$

$$\varepsilon_\theta = \frac{u}{r} \tag{5}$$

$$\varepsilon_r = \frac{\partial u}{\partial r} \tag{6}$$

Use the displacement potential function to represent radial displacement and put it into Eq. (1), we can obtain:

$$\frac{\partial}{\partial r}\frac{\partial^2 \Phi}{\partial t^2} = \frac{2G+\lambda}{\rho}\frac{\partial}{\partial r}\left(\frac{\partial^2 \Phi}{\partial r^2} + \frac{1}{r}\frac{\partial \Phi}{\partial r}\right) \tag{7}$$

Take the squeezing wave velocity as the compressional wave speed $c_p = \sqrt{\frac{2G+\lambda}{\rho}}$ and put it into Eq. (7) and integrating can obtain:

$$\frac{\partial^2 \Phi}{\partial t^2} = c_p^2\left(\frac{\partial^2 \Phi}{\partial r^2} + \frac{1}{r}\frac{\partial \Phi}{\partial r}\right) \tag{8}$$

The approximate general solution for Eq. (8) is:

$$\Phi(r,t) = \frac{1}{\sqrt{r}} f\left(\frac{r}{c_p} - t\right) \tag{9}$$

$$u(r,t) = \frac{\partial \Phi}{\partial t} = -\frac{1}{2} r^{-\frac{3}{2}} f + \frac{1}{c_p} r^{-\frac{1}{2}} f' \tag{10}$$

$$\frac{\partial u}{\partial t}(r,t) = \frac{1}{2} r^{-\frac{3}{2}} f' - \frac{1}{c_p} r^{-\frac{1}{2}} f'' \tag{11}$$

$$\frac{\partial^2 u}{\partial t^2}(r,t) = -\frac{1}{2} r^{-\frac{3}{2}} f'' + \frac{1}{c_p} r^{-\frac{1}{2}} f''' \tag{12}$$

$$\varepsilon_r = \frac{3}{4} r^{-\frac{5}{2}} f - \frac{1}{c_p} r^{-\frac{3}{2}} f' + \frac{1}{c_p^2} r^{-\frac{1}{2}} f'' \tag{13}$$

$$\varepsilon_\theta = -\frac{1}{2} r^{-\frac{5}{2}} f + \frac{1}{c_p} r^{-\frac{3}{2}} f' \tag{14}$$

$$\varepsilon_r + \varepsilon_\theta = \frac{\partial^2 \Phi}{\partial r^2} + \frac{1}{r}\frac{\partial \Phi}{\partial r} = \frac{1}{c_p^2}\frac{\partial^2 \Phi}{\partial t^2} \tag{15}$$

Combining Eq. (4), the radial positive stress obtained is:

$$\sigma_r = (2G+\lambda) r^{-\frac{1}{2}} \frac{1}{c_p^2} f'' - 2G\left(\frac{1}{c_p} r^{-\frac{3}{2}} f' - \frac{1}{2} r^{-\frac{5}{2}} f\right) \tag{16}$$

Comparing with Eq. (10), we can obtain:

$$\sigma_r = (2G+\lambda) r^{-\frac{1}{2}} \frac{1}{c_p^2} f'' - \frac{2G}{r} u \tag{17}$$

$$\frac{\partial \sigma_r}{\partial t} = -(2G+\lambda) r^{-\frac{1}{2}} \frac{1}{c_p^2} f''' - \frac{2G}{r}\frac{\partial u}{\partial t} \tag{18}$$

Synthesizing the Eq. (12, 17, 18), we obtain

$$\sigma_r + \frac{2r}{c_p}\frac{\partial \sigma_r}{\partial t} = -\frac{2G}{r}u - \frac{4G}{c_p}\frac{\partial u}{\partial t} - 2r\rho\frac{\partial^2 u}{\partial t^2} \tag{19}$$

We simulate Eq. (19) with spring, damper and mass unit system, as shown in **Figure 3**.

Dynamic equilibrium differential equations are listed in the mechanical model as shown in **Figure 2**:

$$ku_1 + c(\dot{u}_1 - \dot{u}_2) = -f(t) \tag{20}$$

$$m\ddot{u}_2 + c(\dot{u}_2 - \dot{u}_1) = 0 \tag{21}$$

where u_1、u_2 represent two degrees of freedom of the displacement and $f(t)$ represents the force applied to the boundary point.

Replace the Eq. (20) into (21) to get:

$$f + \frac{m}{c}f' = -ku_1 - \frac{mk}{c}\dot{u}_1 - m\ddot{u}_1 \tag{22}$$

In contrast, the factor of the element is obtained by analogy:

$$m = 2\rho r, \quad c = \rho c_p, \quad k = \frac{2G}{r} \tag{23}$$

For the mechanical model in **Figure 2**, neglecting the quality and fixing on the end of the mass-connected dampers which can simplify the calculation and improve the accuracy of the calculation results form the spring damping element in **Figure 3**, which can be easily combined with large general-purpose finite element software.

2.2. The two- and three-dimensional spring damping coefficient

The derivation is based on the spring damping coefficient obtained by the P-wave. Similarly, there is a similar coefficient form for the shear wave.

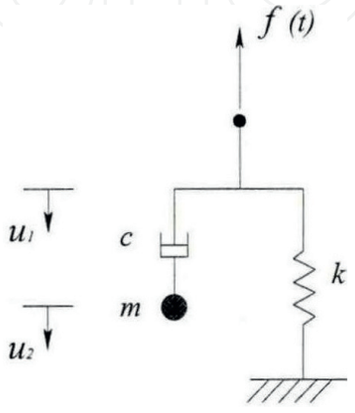

Figure 2. Viso-spring model.

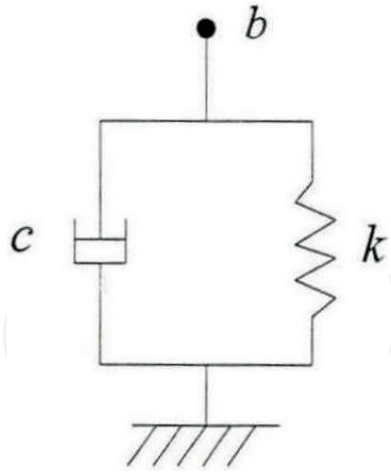

Figure 3. Viso-spring component.

The damping coefficients of the two- and three-dimensional viscoelastic artificial boundaries are summed up.

Two dimension:

Compressional wave (P-wave):

$$k = \frac{2G}{r}, \quad c = \rho c_p \tag{24}$$

Shear wave (SV, SH wave):

$$k = \frac{2G}{r}, \quad c = \rho c_s \tag{25}$$

Three dimension:

Compressional wave (P-wave):

$$k = \frac{4G}{r}, \quad c = \rho c_p \tag{26}$$

Shear wave (SV, SH wave):

$$k = \frac{2G}{r}, \quad c = \rho c_s \tag{27}$$

Based on the Eqs. (24)–(27) the damping coefficient of spring is summed up as follows:

$$K = \alpha \frac{G}{r} \sum_{i=1}^{n} A_i, \quad C = \rho c \tag{28}$$

where k c are the spring damping coefficients at the boundary; r is the distance from the scattering wave to the boundary; ρ and G are the medium density and the shear modulus,

Type	Direction	α
Two-dimensional viscoelastic artificial boundary	Normal direction in plane	2.0
	Tangential direction in plane	1.5
	Tangential direction out of plane	0.5
Three-dimensional viscoelastic artificial boundary	Normal direction	4.0
	Tangential direction	2.0

Table 1. The visco-elastic artificial boundary parameter α.

respectively, c is the wave velocity in the medium where the P-wave velocity c_p and the S-wave velocity c_s are the P-wave velocity and the S-wave velocity in the normal and the tangential direction, respectively. $\sum_{i=1}^{n} A_i$ is the area represented by a boundary node obtained by *arnode* function in ANSYS. The value of the parameter α can be found in the **Table 1**.

3. Input method of equivalent load fluctuation

Liu Jingbo introduced a method for seismic waves that are converted to the equivalent load seismic waves on the viscoelastic artificial boundary to conduct wave inputs. The method calculating structural seismic responses by the combination of viscoelastic artificial boundary and large general-purpose finite element program can be summed up in five steps in the earlier flowchart [19].

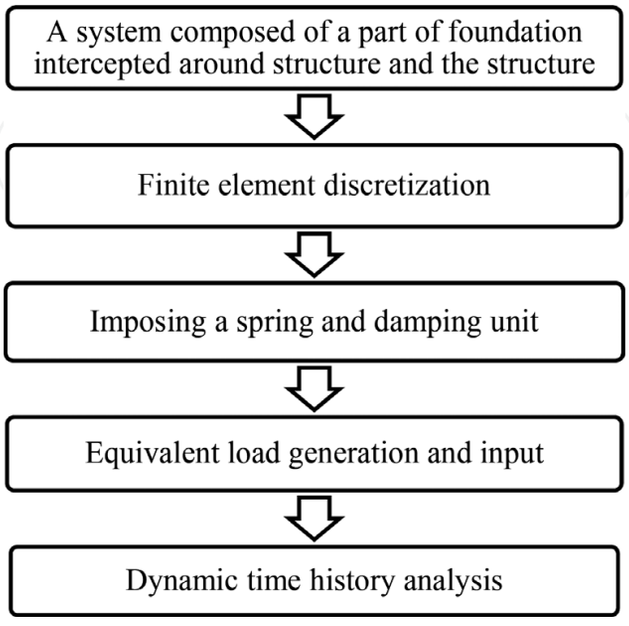

http://dx.doi.org/10.5772/intechopen.76619

3.1. Wave field separation

The total field displacement U_b^t is decomposed into the incident field U_b^f (including incidence and reflection) and scattering field U_b^s, as shown in **Figure 1**.

$$\begin{bmatrix} M_s & \\ & M_b \end{bmatrix} \begin{bmatrix} \ddot{U}_s \\ \ddot{U}_b^t \end{bmatrix} + \begin{bmatrix} C_{ss} & C_{sb} \\ C_{bs} & C_{bb}+C \end{bmatrix} \begin{bmatrix} \dot{U}_s \\ \dot{U}_b^t \end{bmatrix} + \begin{bmatrix} K_{ss} & K_{sb} \\ K & K_{bb}+K \end{bmatrix} \begin{bmatrix} U_s \\ U_b^t \end{bmatrix} = \begin{bmatrix} 0 \\ \tau_0 \end{bmatrix} \tag{29}$$

$$\begin{bmatrix} M_s & \\ & M_b \end{bmatrix} \begin{bmatrix} \ddot{U}_s \\ \ddot{U}_b^t \end{bmatrix} + \begin{bmatrix} C_{ss} & C_{sb} \\ C_{bs} & C_{bb} \end{bmatrix} \begin{bmatrix} \dot{U}_s \\ \dot{U}_b^t \end{bmatrix} + \begin{bmatrix} K_{ss} & K_{sb} \\ K & K_{bb} \end{bmatrix} \begin{bmatrix} U_s \\ U_b^t \end{bmatrix} = \begin{bmatrix} 0 \\ \tau_0 - C\dot{U}_b^t - KU_b^t \end{bmatrix} \tag{30}$$

Equivalent load is $F_e = \tau_0 - C\dot{U}_b^t - KU_b^t$, in this, $U_b^t = U_b^f + U$, and if we take one derivative of this we get $\dot{U}_b^t = \dot{U}_b^f + \dot{U}$. Equivalent load becomes $F_e = \tau_0 - C\dot{U}_b^f - KU_b^f - C\dot{U}_b^s - KU_b^s$; the scattering field fluctuation will be absorbed by the yellow damping unit and the general expression of the equivalent load will be obtained, and it is $F_e = \tau_0 - C\dot{U}_b^f - KU_b^f$.

3.2. Equivalent load input

Equivalent load expression is $F_e = KU + C\dot{U} + \tau_0$; note $KU + C\dot{U}$ as the velocity displacement term and τ_0 as the stress term.

As shown in **Figure 4**, through the stress analysis of the microelement on the boundary, we obtained in the first stress state, the Poisson effect of the cell is considered, and the shear stress in the second stress state is equal to each other. Therefore, the lateral boundary stress τ_0 caused by seismic waves can be discussed on two situations of P-wave and S-wave (wave vertical incidence).

The stress when P-wave enters the lower boundary: $\tau_0 = \frac{\nu\rho C_p \dot{U}_b^f}{1-\nu.}$

The stress when S-wave enters the lower boundary: $\tau_0 = \rho C_s \dot{U}_b^f$

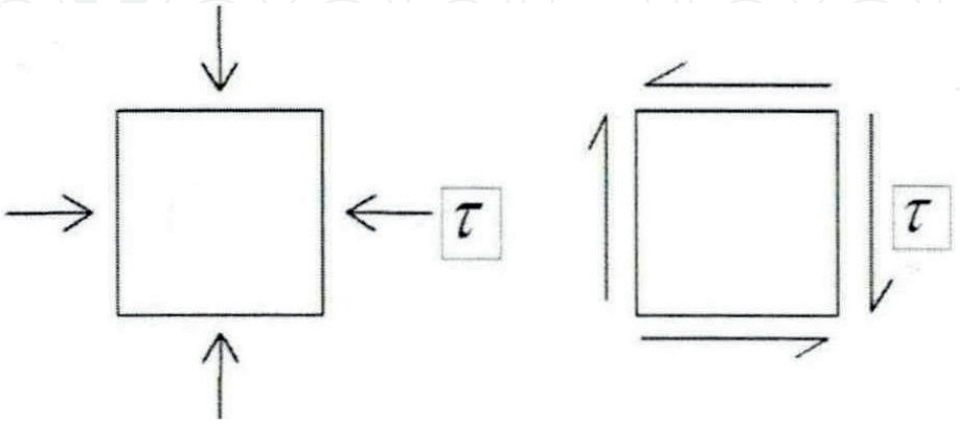

Figure 4. Soil element at the boundary.

3.2.1. Two-dimensional equivalent load input

The value of the spring damping coefficient is based on "a direct method of the analysis of the dynamic interaction of the structural foundation" [6, 9], and the specific values are:

Surface normal: $k_N = \frac{G}{2r}\sum A, \quad C_N = \rho C_p \sum A$

Surface tangential: $k_T = \frac{G}{2r}\sum A, \quad C_T = \rho C_s \sum A$

where k_N is the coefficient of the normal spring coefficient, C_N is the coefficient of the normal damper, k_T represents the tangential spring coefficient and C_T is the coefficient of the tangential damper.

The spring damping coefficients of each boundary and the direction of the velocity displacement and stress in the equivalent load of each boundary line when seismic waves are inputs from two directions are given as shown in **Figure 5**.

The boundary line 1:

The spring damper coefficient:

Surface normal (external normal Y, minus): $k_N = \frac{G}{2r}\sum A, \quad C_N = \rho C_p \sum A$

Surface tangential(X): $k_T = \frac{G}{2r}\sum A, \quad C_T = \rho C_s \sum A$

Equivalent load in all directions (two-way input):

X dimension: Velocity displacement term (X+); stress term (X+)

Y dimension: Velocity displacement term (Y+); stress term (Y+)

The boundary line 2:

The spring damper coefficient:

Surface normal (external normal X, plus): $k_N = \frac{G}{2r}\sum A, \quad C_N = \rho C_p \sum A$

Surface tangential(Y): $k_T = \frac{G}{2r}\sum A, \quad C_T = \rho C_s \sum A$

Equivalent load in all directions (two-way input):

X dimension: Velocity displacement term (X+); stress term (X−)

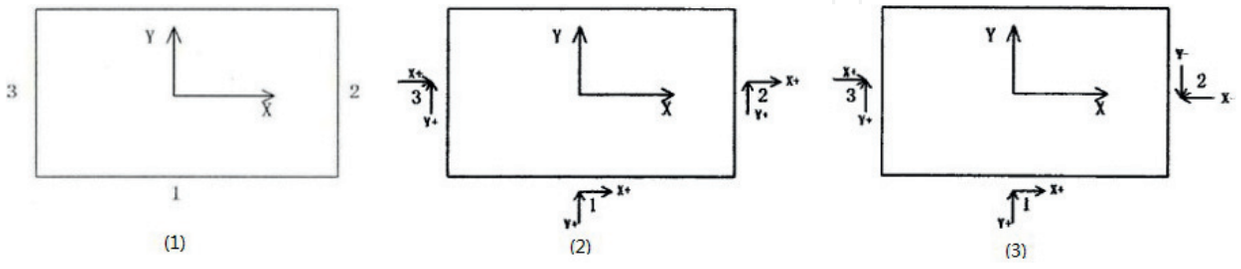

Figure 5. The input of equivalent load in two dimensions. (1) Two-dimensional numbering schematic. (2) Input of equivalent load term. (3) Input of stress term.

Y dimension: Velocity displacement term (Y+); stress term (Y−)

The boundary line 3:

The spring damper coefficient:

Surface normal (external normal X, minus): $k_N = \frac{G}{2r}\sum A, \quad C_N = \rho C_p \sum A$

Surface tangential(Y): $k_T = \frac{G}{2r}\sum A, \quad C_T = \rho C_s \sum A$

Equivalent load in all directions (two-way input):

X dimension: Velocity displacement term (X+); stress term (X−)

Y dimension: Velocity displacement term (Y+); stress term (Y−)

3.2.2. Three-dimensional equivalent load input

As shown in the three-dimensional model of **Figure 6**, the coordinate system is in conformity with the laws of the corkscrew, the "1" is the bottom, the "2" is the front interface, the "3" is the right side of the boundary surface, the "4" is the back interface and the "5"is the left side of the boundary surface, and the faces from 2 to 5 are numbered counter-clockwise.

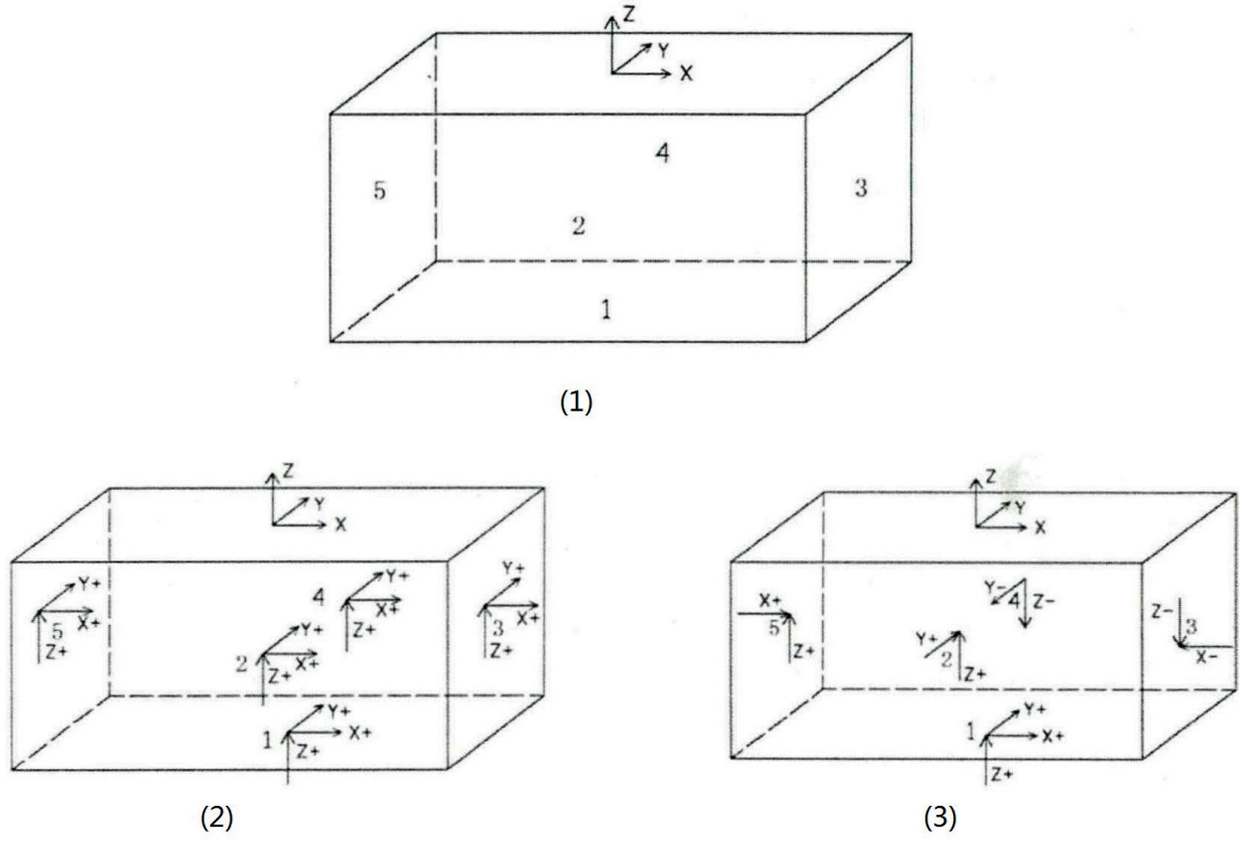

Figure 6. The input of equivalent load in three dimensions. (1) Three-dimensional numbering diagram. (2) Input of equivalent load term. (3) Input of stress term.

The value of the spring damping coefficient is based on "three-dimensional time-domain viscoelastic artificial boundary in wave problem" [7, 10], and the specific values are:

Face normal: $k_N = \frac{4G}{r}\sum A, \quad C_N = \rho c_p \sum A$

Surface tangential: $k_T = \frac{2G}{r}\sum A, C_T = \rho c_s \sum A$

where k_N is the coefficient of the normal spring coefficient, C_N is the coefficient of the normal damper coefficient, k_T represents the tangential spring coefficient and C_T is the coefficient of the tangential damper.

The spring damping coefficients of each boundary and the direction of the velocity displacement and stress in the equivalent load of each boundary line when seismic waves are inputs from three directions are given as shown in **Figure 6**.

Face 1:

The spring damper coefficient:

Surface normal (external normal Z, minus): $k_N = \frac{4G}{r}\sum A, c_N = \rho c_p \sum A$

Surface tangential (XY): $k_T = \frac{2G}{r}\sum A$, $c_T = \rho c_s \sum A$.

Equivalent load in all directions (three-way input):

X dimension: Velocity displacement term (X+); stress term (X+)

Y dimension: Velocity displacement term (Y+); stress term (Y+)

Z dimension: Velocity displacement term (Z+); stress term (Z+)

Face 2:

The spring damper coefficient:

Surface normal (external normal Y, minus): $k_N = \frac{4G}{r}\sum A, c_N = \rho c_p \sum A$

Surface tangential (XZ): $k_T = \frac{2G}{r}\sum A$, $c_T = \rho c_s \sum A$.

Equivalent load in all directions (three-way input):

X dimension: Velocity displacement term (X+); stress term (nothing)

Y dimension: Velocity displacement term (Y+); stress term (Y+)

Z dimension: Velocity displacement term (Z+); stress term (Z+)

Face 3:

The spring damper coefficient:

Surface normal (external normal X, plus): $k_N = \frac{4G}{r}\sum A, c_N = \rho c_p \sum A$

Surface tangential (YZ): $k_T = \frac{2G}{r}\sum A, \quad c_T = \rho c_s \sum A$.

Equivalent load in all directions (three-way input):

X dimension: Velocity displacement term (X+); stress term (X-)

Y dimension: Velocity displacement term (Y+); stress term (nothing)

Z dimension: Velocity displacement term (Z+); stress term (Z-)

Face 4:

The spring damper coefficient:

Surface normal (external normal Y, plus): $k_N = \frac{4G}{r}\sum A, c_N = \rho c_p \sum A$

Surface tangential (XZ): $k_T = \frac{2G}{r}\sum A, \quad c_T = \rho c_s \sum A.$

Equivalent load in all directions (three-way input):

X dimension: Velocity displacement term (X+); stress term (nothing)

Y dimension: Velocity displacement term (Y+); stress term (Y-)

Z dimension: Velocity displacement term (Z+); stress term (Z-)

Face 5:

The spring damper coefficient:

Surface normal (external normal X, minus): $k_N = \frac{4G}{r}\sum A, c_N = \rho c_p \sum A$

Surface tangential (XZ): $k_T = \frac{2G}{r}\sum A, \quad c_T = \rho c_s \sum A.$

Equivalent load in all directions (three-way input):

X dimension: Velocity displacement term (X+); stress term (X+)

Y dimension: Velocity displacement term (Y+); stress term (nothing)

Z dimension: Velocity displacement term (Z+); stress term (Z+)

3.2.3. The free field motion considering the traveling wave effect

$$u(k,t) = \begin{cases} u_{inp}(k,t) & t \le \dfrac{d}{c} \\ u_{inp}(k,t) + u_{ref}\left(k, t - \dfrac{2H-d}{c}\right) & \dfrac{d}{c} < t < t_{end} \\ u_{ref}\left(k, t - \dfrac{2H-d}{c}\right) & t \ge t_{end} \end{cases} \tag{31}$$

where k represents a point at the boundary point, d represents the vertical distance from the bottom boundary point k, c represents the velocity of wave propagation, u_{inp} and u_{ref} represent the displacement wave and the displacement wave displacement, respectively.

In the process of wave propagation in elastic medium, deformation, stress and particle will spread at the same speed in the same way. The boundary point K at a certain time is the superposition of the incident wave displacement and the reflected wave displacement. This is similar for velocity.

4. Seismic input model of slope site constructed by virtual symmetry substructure

4.1. Equivalent load of node in slope site

As in **Figure 7**, the normal direction of the two sides with different heights is fixed in the direction of X, considering the traveling wave effect that the expression of the equivalent load on the two sides of the slope is:

$$\sigma_x = K\left(u_{inp}(k,t) + u_{ref}\left(k, t - \frac{2H-d}{c}\right)\right) + C\left(u_{inp}(k,t) + u_{ref}\left(k, t - \frac{2H-d}{c}\right)\right) \tag{32}$$

$$\sigma_{x高} = K\left(u_{inp}(k,t) + u_{ref}\left(k, t - \frac{2H_1-d}{c}\right)\right) + C\left(u_{inp}(k,t) + u_{ref}\left(k, t - \frac{2H_1-d}{c}\right)\right) \tag{33}$$

$$\sigma_{x低} = K\left(u_{inp}(k,t) + u_{ref}\left(k, t - \frac{2H_2-d}{c}\right)\right) + C\left(u_{inp}(k,t) + u_{ref}\left(k, t - \frac{2H_2-d}{c}\right)\right) \tag{34}$$

For (7), take $\Delta t = \frac{2H_1-2H_2}{c}$, so

$$\sigma_{x低} = K\left(u_{inp}(k,t) + u_{ref}\left(k, t - \frac{2H_1-d}{c} + \Delta t\right)\right) + C\left(u_{inp}(k,t) + u_{ref}\left(k, t - \frac{2H_1-d}{c} + \Delta t\right)\right) \tag{35}$$

where K and C are the coefficient of spring dampers, and the other symbolic meanings are the same as (s4).

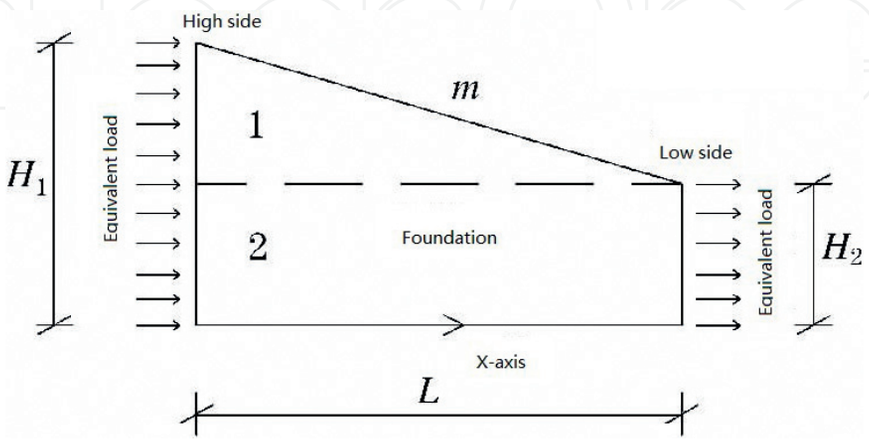

Figure 7. Equivalent load on the slope site.

Comparing Eqs. (33) and (35), the difference is Δt between the displacement and velocity time history which causes the difference in the size of the two side nodes with different heights. The ground is artificially divided into one and two parts in **Figure 3**, and the reasons for the inconsistency of the equivalent load can be seen directly. Part 1 has only boundaries without the corresponding equivalent load. The force is equal to the product of the stress and the area, and steeper the slope, the greater the difference between the area of two sides; the difference of the force will be more obvious.

4.2. The solving steps of the virtual symmetric substructure system

The analysis of the expression of the equivalent load shows that the difference in height and area can cause the inconsistency of the equivalent load of the two sides. By analyzing the mechanical properties, we can come to a conclusion that the cause of displacement divergence or response eccentricity is the inconsistency of the equivalent load resultant force in the two sides with different heights. Therefore, a virtual symmetric substructure is used to construct a viscoelastic artificial boundary seismic input model suitable for the slope site; the specific steps are as follows:

1. As shown in **Figure 8**, the boundary of the symmetry system composed by the original slope model and an existing nominally only equal-sized slope foundation about line 2 is line 1 and 3 based on two dimensions. Based on the high consistency of the boundary line, the equivalent load generation and input method of the flat site can be directly applied to calculate the seismic response in this case, and the node displacement and velocity on line 2 of the symmetry axis can be extracted.

2. Calculate the equivalent load of the node of line 2; only the actual slope is calculated that the virtual foundation is canceled where the boundary line is changed into line 1 and 2. The displacement and velocity of nodes extracted from step (1) are the total displacement and total velocity at any time that we do not need to consider the traveling wave effect, so the formula for calculating the equivalent load is: $F_e = \dot{C}U_{tb} + KU_b^t$. Take the calculated equivalent load of the line 2 node and the equivalent load of the original line 1 into the slope model to calculate the seismic response of the structure.

The steps for solving the three-dimensional slope model are the same as earlier. In theory, the equivalent load of this structure is equal on the boundary line, and it can effectively simulate the wave propagation.

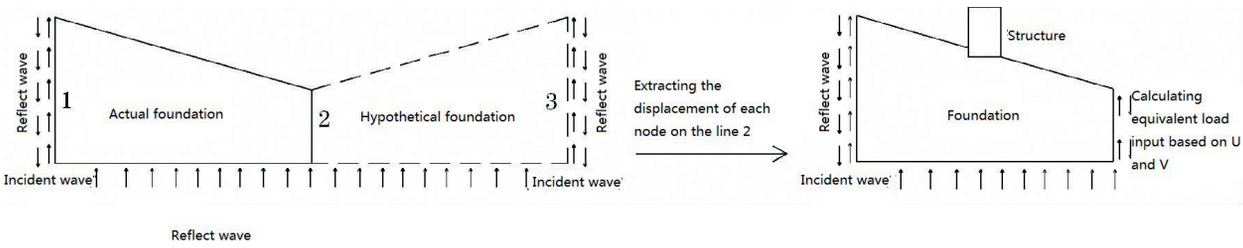

Figure 8. Sketch of recommended seismic input mode.

5. Example

5.1. Input seismic waves to the free field from three directions

Firstly, the correctness of the three-dimensional viscoelastic boundary procedure under the conditions of free field is verified, namely, the surface displacement analytical solution of the homogeneous free field is two times than the incident displacement time history when considering the delay due to the traveling wave effect. The seismic input from 3 directions all is simple harmonic sine wave. Input two cycles, and view the stability of the result.

The model is a cuboid, the length and width of it are 800 m, the height of it is 400 m and the size is shown in **Figure 9**. The shear modulus is 5.292×10^9 Pa, the Poisson ratio is 0.25, the density is 2700 kg/m^3 and the shear wave velocity is 1400 m/s. The type of the solid unit is solid45, size of the unit is 40 m and three-dimensional spring damping unit Combin14 on the bottom boundary and four side boundaries is applied. The coordinate origin is selected at the center point of the top surface and is taken as the observation point, marked O.

As shown in **Figure 10**, P wave's velocity is greater than S wave's and reaches the top after 0.180 s; it has simple harmonic vibration with the size as twice as the bottom input, and at the same time the response of the S wave is affected; S wave shows slight fluctuations between 0.180 and 0.285 s and then is followed by a twofold unit sinusoidal vibration. The response of the top of the three directions is two times than the bottom input, and the displacement responses of the x direction and y direction are basically the same. We verify the correctness of the seismic input method and the procedure and then study the seismic response under the slope.

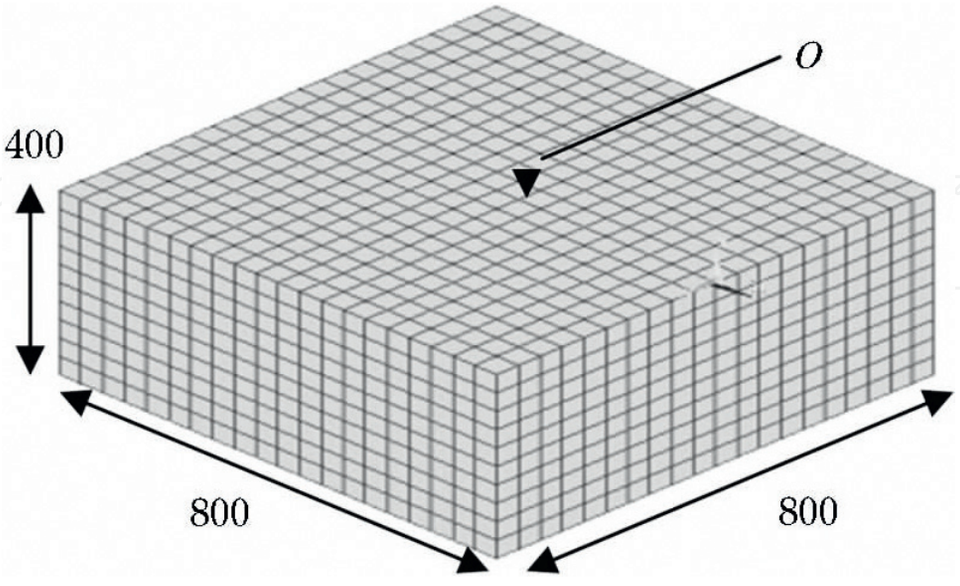

Figure 9. Three dimensional finite element model of free-field.

5.2. Input the one-way ground motion in slope field

In order to make a comparison with the method of the symmetrical substructure system, the equivalent load is generated in the form of a flat free field, and the slope model is directly taken as the input to calculate it is seismic response. The slope model (**Figure 11**) is selected and there

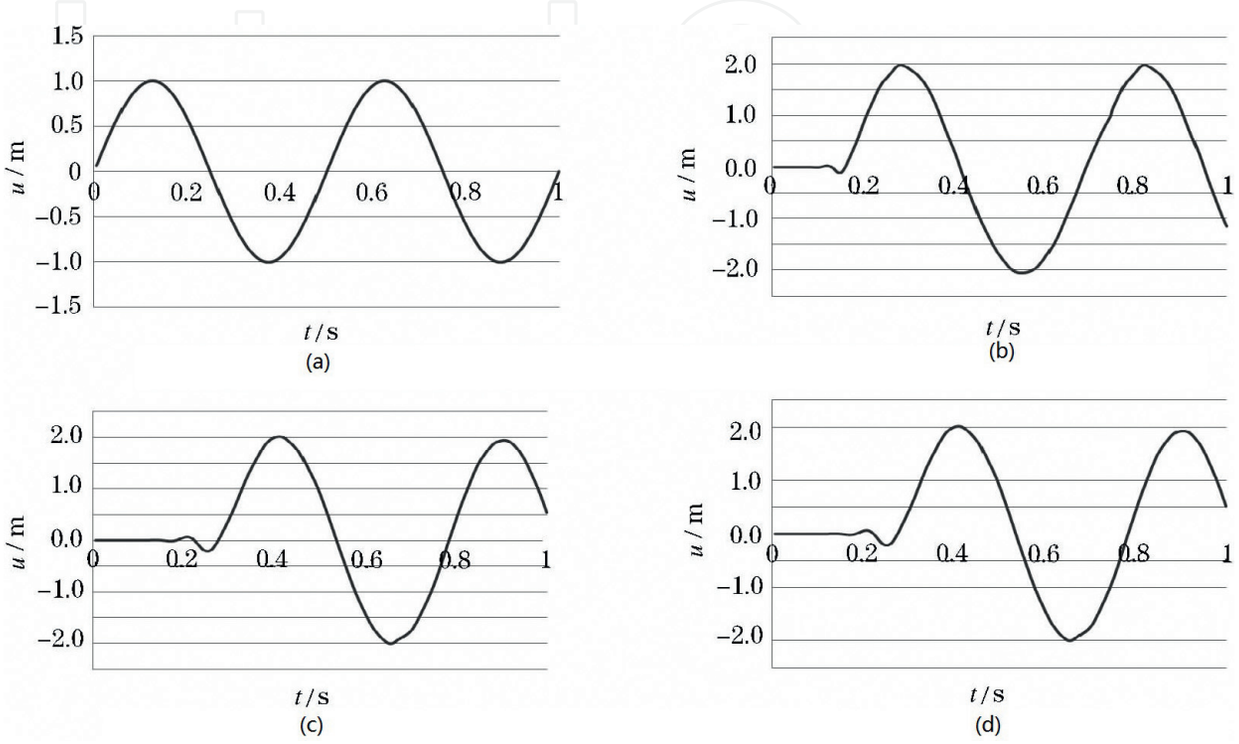

Figure 10. Dynamic responses of free-field. (a) The unit sine wave entered at the bottom. (b) The z-directional displacement time history of the observation point O (P-wave, α-angle). (c) The x-directional displacement time history of the observation point O (S-wave, α-angle). (d) The y-directional displacement time history of the observation point O (S-wave, α-angle).

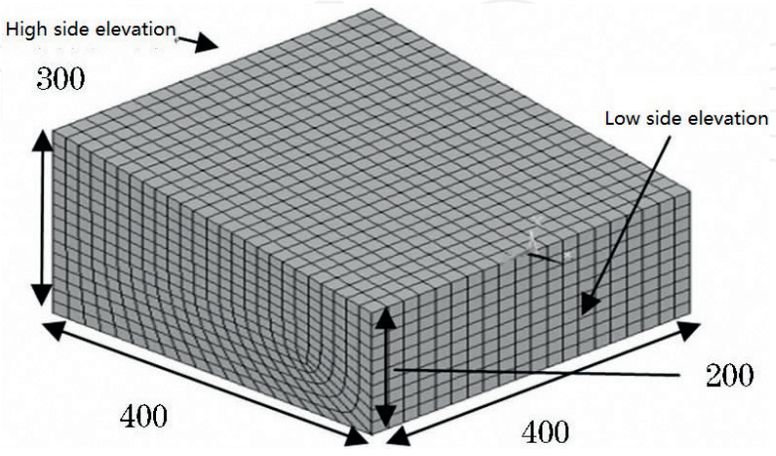

Figure 11. The map of finite element grid division of slope.

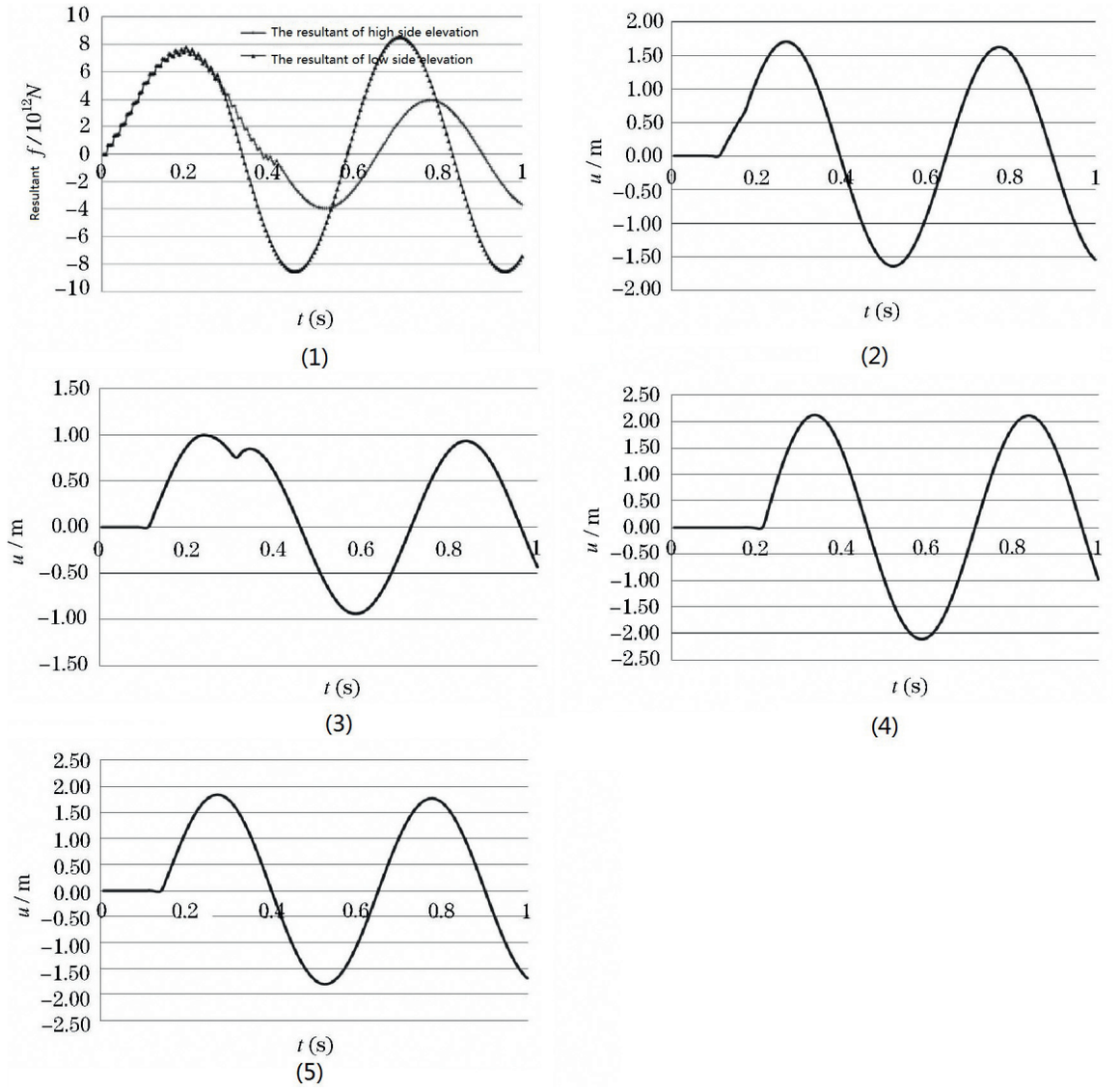

Figure 12. Dynamic responses of slope site. (1) The comparison of the resultant force on the side elevation. (2) The displacement time history of lower side elevation at the height of 160 m. (3) The displacement time history of higher side elevation at the height of 160 m. (4) Vertex displacement time history higher side elevation. (5) Vertex displacement time history higher side elevation.

is a high difference in the side elevation of one direction. The base is square and the length and width is 400 m. Take the normal direction on both sides of the plane as the X-axis, and so, the height of both sides in X is 300 and 200 m, respectively, and gradient of the slope is 0.25; the detailed dimensions are shown in the figure. The material parameters are the same as the free field. The entity unit type is solid45, the size of the element is 20 m in the direction of the boundary line; the mapping subdivision is performed within the surface. We apply a three-dimensional spring damping unit Combin14 on the bottom boundary and four side boundaries. In order to clearly see the change of equivalent load force, only input the unit sinusoidal shear wave in X; the waveform is the same as the input of the three-dimensional free-field calculation example.

As **Figure 12** shows:

1. In **Figure 12 (1)**, after 0.25 s, the equivalent load in x of the low-side elevation is far greater than that of the high-side elevation, and the resultant force is unbalanced.

2. Compared with the two points with elevation of 160 m in two sides, the distance time history between the two points is completely different, as shown in **Figure 12 (2)** and **(3)**. The displacement of **Figure 12 (2)** presents obviously the change of the cycle which is led by the superposition, the amplitude is 1, and **Figure 12 (3)** shows the complete sinusoidal waveform with the amplitude of 1.72. Furthermore, the displacement time history of the vertex on both sides of the elevation is further compared to see the accuracy and stability of the results. In **Figure 12 (4)**, the displacement amplitude of the first period is 2.16, the displacement amplitude of the second period is 2.19, showing an increasing trend and faring from the relationship of two times. In **Figure 12 (5)**, the displacement amplitude of the first period is 1.76, the displacement amplitude of the second period is 1.73 and we see a decrease.

3. So you can see that the model is biased towards one side; in this chapter, it is considered that the imbalance of the overall resultant force of the model leads to this eccentricity. Presumably, this eccentricity is more apparent when the slope is larger. Because the seismic wave calculating actually is not a regular periodic wave, so directly taking the equivalent load calculated by flat free field into the slope site model will cause the eccentricity, or even wrong results.

5.3. The slope site model is calculated using a symmetric substructure

In accordance with the method recommended in Section 2 and the slope model, the model size is the same and the material parameters are unchanged. According to step (1), a symmetric system is constructed by setting phonily the isometrical foundation and the finite element mesh of the symmetric model is shown in **Figure 13**. The height of the symmetric face of the model is 200 m, the height of the two sides is 300 m, the base length is 800 m and the width is

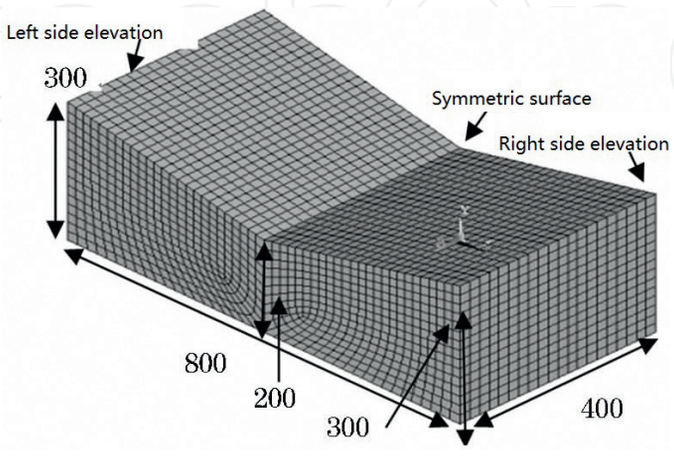

Figure 13. Mesh division of finite element of symmetrical model.

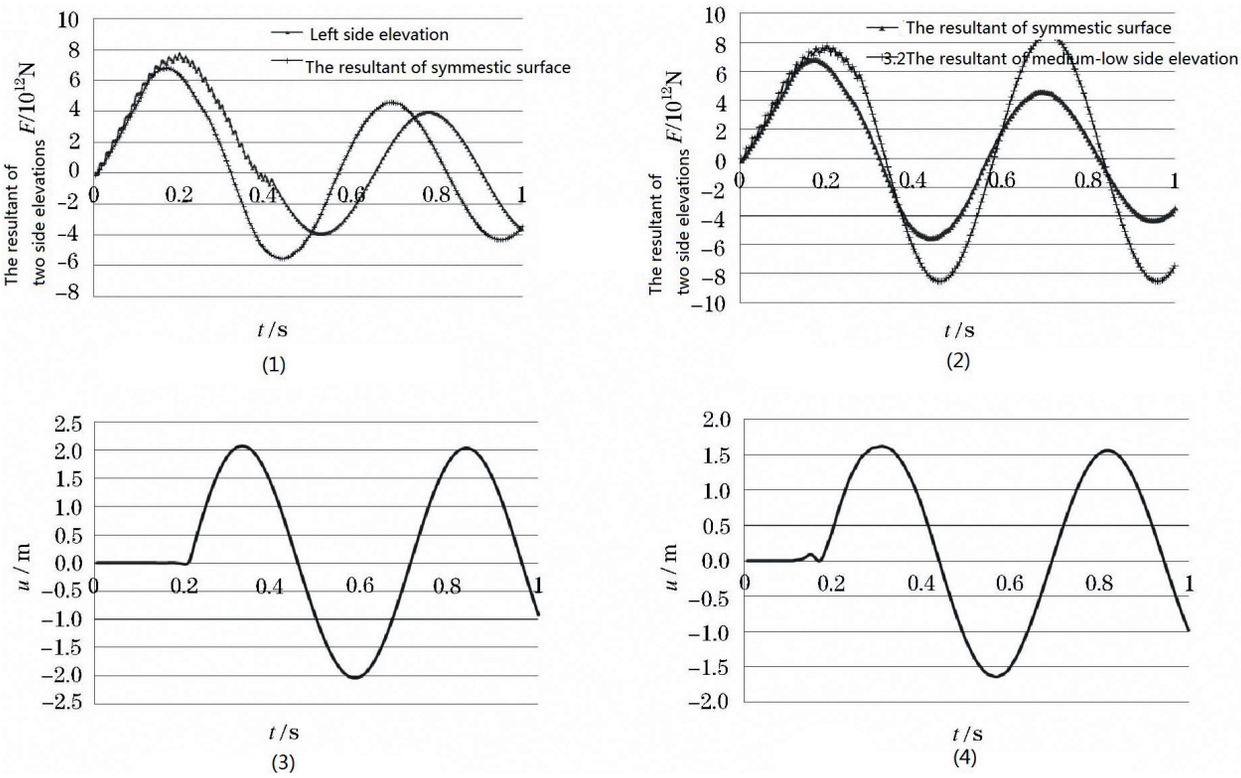

Figure 14. Dynamic response of symmetrical model. (1) Resultant force contrast between symmetry plane and left side elevation. (2) Resultant force contrast between symmetry plane and low side elevation. (3) Displacement time history of the vertex of left side elevation. (4) Displacement time history of the point with the height of 250 m.

400 m. The solid unit of Solid45 is used to divide the grid, and the size of the finite element mesh on the boundary line is 20 m, with a total of 23,876 units. The model in step (2) is the same as **Figure 11**. Since the symmetrical face in step (1) is the same face as the low side elevation of the slope model in step (2), they will be replaced by symmetry plane in the following.

Figure 14 (1) is the contrast diagram of the equivalent load force of every moment of the symmetry plane and the equivalent load of the left side. **Figure 14 (2)** is the contrast diagram of the equivalent load force of the symmetry plane and the equivalent load of the low-side elevation in Section 2.

You can see from **Figure 14**:

1. The equivalent load size of the symmetrical face in **Figure 14 (1)** is close to that of the left elevation, and the change of equivalent load conforms to the theoretical expectation. As shown in **Figure 14 (2)**, the numerical variation of the resultant force of the lower lateral equivalent load of the slope model is significant, indicating the effectiveness of the proposed method.

2. In **Figure 14 (3)** and **(4)**, the displacement time history is numerically stable and the rationality of the seismic input mode of constructing the symmetric substructure is proved from the results.

6. Conclusion

In this chapter, an earthquake input mode for viscoelastic artificial boundary under the condition of the slope is proposed by constructing the virtual symmetric substructure system. The numerical examples verify the stability of the results and the following conclusions are obtained:

1. Based on the numerical expression of the equivalent load at the viscoelastic artificial boundary, the chapter deduces that the height and area difference of the side elevation are the important reasons for the inconsistency of the seismic input load.
2. By constructing a virtual symmetric structure system, we can ensure the symmetry of foundation calculation area outside the boundaries, which is easy to simulate the propagation characteristics of the free field seismic waves and determine the external boundary input load.
3. The method ensures the accordance of resultant force of seismic input load in the condition of the slope field, makes the dynamic response results more reasonable and is easy to implement in a large general finite element software-ANSYS and can be used in the analysis of seismic responses of the nuclear structure under the conditions of two-dimensional and three-dimensional slope field.

Author details

Li Jianbo* and Liu Weihong

*Address all correspondence to: jianboli@dlut.edu.cn

Institute of Earthquake Engineering, Dalian University of Technology, Dalian, China

References

[1] Liao ZP. Introduction to Wave Motion Theories in Engineering. Beijing: Science Press; 2002

[2] Du X. Theories and Methods of Wave Motion for Engineering. Beijing: Science Press; 2009

[3] Lysmer J, Kulemeyer RL. Finite dynamic model for infinite media. Journal of Engineering Mechanics, ASCE. 1969;**95**(4):759-877

[4] Deeks AJ, Randolph MF. Axisymmetric time-domain transmitting boundaries. Journal of Engineering Mechanics, CE. 1994;**20**(1):25-42

[5] Liao ZP, Wong HL. A transmitting boundary for the numerical simulation of elastic wave in stratified media. Computers in Physics. 1992;**101**:386-418

[6] Liao ZP. Guidance of Engineering Wave Theory. 2nd ed. BeiJing: Science press; 2002

[7] Du X, Zhao M. Analysis method for seismic response of arch dams in time domain based on viscous-spring artificial boundary condition. SHUI LI XUE BAO. 2006;**37**(9):1063-1069

[8] Du X, Zhao M. A local time-domain transmitting boundary for simulating cylindrical elastic wave propagation in infinite media. Soil Dynamics and Earthquake Engineering. 2010;**30**:937-946

[9] Liu J, Lv Y. A direct method for the analysis of dynamic interaction of structural foundations. China Civil Engineering Journal. 1998;**31**(3):55-64

[10] Liu J, Wang Z, Du X, et al. Three-dimension visco-elastic artificial boundaries in domain for wave motion problems. Engineering Mechanics. 2005;**22**(6):46-51

[11] Zhi F. Dynamic response and artificial boundary analysis in soil structure interaction system. Chinese Quarterly of Mechanics. 2009;**30**(3):475-480

[12] Deeks AJ, Randolph MF. Axisymmetric time-domain transmitting boundaries. Journal of Engineering Mechanics, ASCE. 1994;**120**(1):25-42

[13] Liu J, Li B. Three-dimensional viscoelastic static power unified artificial boundary. Chinese science E. 2005;**35**(9):996-980

[14] Lu H, Liang Y, Shouping S. Calculation and analysis of dynamic interaction system of pile foundation structure on layered foundation. Journal of Geotechnical Engineering. 2007; **29**(5):701-711

[15] Gao F, Fengbing Z. Study on artificial boundary conversion method for static and dynamic analysis of underground structures. Vibration and Shock. 2011;**30**(11):165-170

[16] Xue Z, Pei Q, Wu S, et al. Input seismic motion based on the viscous-spring boundary: Analytical solution and numerical simulation. International Journal of u-and eE-Service Science and Technology. 2016;**9**(6):59-68

[17] Jingbo L, Yixin D, Qiushi Y. Visco-elastic and the ground motion input implement in the general finite element software. Journal of Disaster Prevention and Mitigation Engineering. 2007;**27**:37-42

[18] Li J, Chen JY, Lin G. Finite element damping extraction method for dynamic interaction time domain analysis of nonhomogeneous unbounded rock. Chinese Journal of Geotechnical Engineering. 2004;**26**(2):263-267

[19] Jiang X, Li J, Lin G. Study on the seismic input mode of viscoelastic artificial boundary under the condition of slope site. World Earthquake Engineering. 2013;**29**(4):126-132